Quantitative Hole Mobility Simulation and Validation in Molecular Semiconductors

Daniel Vong,[†] Tahereh Nematiaram,[‡] Makena A. Dettmann,[†] Tucker L. Murrey,[†] Lucas S. R. Cavalcante,[¶] Sadi M. Gurses,[¶] Dhanya Radhakrishnan,[§] Luke L. Daemen,[∥] John E. Anthony,[⊥] Kristie J. Koski,[§] Coleman X. Kronawitter,[¶] Alessandro Troisi,[‡] and Adam J. Moulé*,[¶]

†*Department of Materials Science and Engineering, University of California Davis, Davis, CA, USA*

‡*Department of Chemistry, University of Liverpool, Liverpool, UK*

¶*Department of Chemical Engineering, University of California Davis, Davis, CA, USA*

§*Department of Chemistry, University of California Davis, Davis, CA, USA*

∥*Oak Ridge National Lab, Oak Ridge, TN, USA*

⊥*University of Kentucky, Lexington, KY, USA*

E-mail: amoule@ucdavis.edu

This is a peer-reviewed, accepted author manuscript of the following article: Vong, Daniel ; Nematiaram, Tahereh ; Dettmann, Makena A, et al. / Quantitative hole mobility simulation and validation in substituted acenes. In: Journal of Physical Chemistry Letters. 2022 ; Vol. 13, No. 24. pp. 5530–5537.

Abstract

Recently, it was proposed that a single long-axis mode dominates the contribution to dynamic disorder (σ) that reduces hole mobility (μ_h), making quenching of this mode a design rule for increased μ_h. To test this hypothesis, we measure and model the full phonon spectrum using multiple spectroscopic techniques and predict the μ_h using σ from the Γ-point only compared to the full Brillouin zone (FBZ). Only inelastic neutron scattering (INS) provides validation of all phonon modes. We found that σ in a set of small molecule semiconductors can be miscalculated by up to 24% when comparing Γ-point against FBZ calculations. A mode analysis shows that many modes contribute to σ and that no single mode dominates. Our results demonstrate the importance of a thoroughly validated phonon calculation, and a need to develop design rules considering the full spectrum of phonon modes.

Graphical TOC Entry

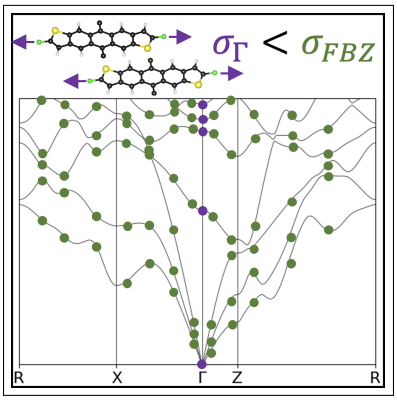

Organic semiconductors (OSC) have undergone rapid development for use in applications such as organic light emitting diodes, transistors, biological and chemical sensors, and wearable and flexible electronics.[1–6] Small molecule OSCs (OSM) have the highest μ among OSCs because they form extended crystalline domains.[7] Planar molecules, like acenes, are natural building blocks for OSC crystals, but they tend to form microdomain boundaries with poor electronic connection across the grain boundaries.[8,9] Decades of study have shown that non-planar organic molecules that employ a central building block consisting of fused aromatic rings with symmetric side chains enable the molecules to:

1. Lock into geometries that may benefit charge transport.[10,11]

2. Form more extended defect free crystalline domains.[12,13]

3. Achieve improved electronic connection through microdomain grain boundaries.[14]

Rubrene, C8-BTBT, C8-DNTT, and TIPS-Pentacene are all examples of substituted acenes that have exhibited high hole mobility (μ_h) of over 1 cm^2/Vs.[15,16]

Examining the charge transport mechanism in OSMs have attracted great attention.[17–21] There is unanimous consensus that μ cannot be computed accurately using either band theory or a hopping mechanism.[22–27] Here we consider the coupling between charge carriers and molecular motions in the framework of transient localization theory (TLT) in order to calculate dynamic disorder (σ). The coupling leads to large transfer integral fluctuations that dynamically localizes the charge carrier on the ps time scale and thereby reduces μ. The coupling between phonons and charge carriers is accounted for using diagonal (intramolecular) and off-diagonal (intermolecular) terms in the Hamiltonian.[24] Recent theory-experiment[16,17,21,28,29] and theory-theory[30–32] studies have shown that TLT provides fairly accurate prediction of μ and trends between molecules.

Recently, μ_hs of several OSMs were calculated based on the spectral measurements of σ.[16,21,33,34] While there is little doubt that the dynamic disorder model correctly accounts for the reduced μ_h, there is disagreement in the literature about how many modes are responsible,

how to measure these modes experimentally, or how to model these modes theoretically. This letter examines this problem using a series of three well studied high μ_h substituted acenes, 6,13-Bis(triisopropylsilylethynyl)(TIPS)-Pentacene, 5,11-Bis(triethylsilylethynyl)anthradithiophene (TESADT), and its fluorinated analogue, diF-TESADT. These molecules form similar crystal structures, yet show a clear increase in μ_h from <1 cm^2/Vs for TIPS-pentacene,[35] to >1 cm^2/Vs in TESADT,[36] and to >6 cm^2/Vs for diF-TESADT.[37] We extend this study beyond brick-wall materials to herringbone type materials, BTBT, C8-BTBT, and Rubrene, some of which were reported to have a single long-axis mode dominating σ.[21] Here we use density functional theory (DFT) coupled to electron-phonon calculations to determine the contribution to σ. We find that all intra- and inter-molecular phonons across the full Brillouin zone (FBZ) contribute to σ, and that no single phonon contributes >10% to σ, regardless of molecular packing. A partial mode analysis is then performed linking the structure-property relationship involving molecular changes and the phonons that contribute to σ.

First we characterize the acoustic and optical phonons using Brillouin scattering (0.1–2 cm^{-1}), inelastic neutron scattering (INS) (3–4000 cm^{-1}), Raman (50–1500 cm^{-1}), and Fourier-transformed infrared (FTIR) (600–1600 cm^{-1}) spectroscopies. Next, we model the crystal using a plane wave DFT supercell that simultaneously and accurately reproduces the measured crystal structure and the phonon spectrum. The electron-phonon coupling is calculated from the DFT model that closely matches the experimental spectrum. Finally, we consider the information contained in each measured spectrum and demonstrate that the isotropic optical spectra not only has missing modes due to selection rules, but also inadequately samples the Brillouin zone, leading to a limited mode analysis and over-assignment of σ. Finally, we compare predictions of μ_h.

We compare four different spectroscopic techniques that measure vibrational modes for TIPS-Pentacene in Fig. 1. The details of the Brillouin scattering result are shown in Fig. S1. In Fig. 1 we also highlight the energy region that is most important for σ on the time scale relevant for μ_h.[17,38,39] This energy region is important because it represents the modes

that are populated at room temperature and could thus contribute to σ. Brillouin scattering (maroon) measured the acoustics modes of the molecule. Although the long-axis acoustic mode has been shown to predict μ_h based on Boltzmann transport in OSMs with plane mirror symmetry,[40] the acoustic modes measured by Brillouin scattering are too low in energy to affect charge transport and high energy vibrations on individual molecules to not affect the ground state energy surface that carries charge. The INS spectrum (black) measures a much higher density of low energy modes over a more complete energy range than either Raman (red) or FTIR (blue), due to optical selection rules. The experimental energy range that Raman can access is limited and many of the lower energy vibrational modes that contain the timescales considered most important for charge transport cannot be resolved. Literature measurements of low-energy Raman (lower than we could obtain) measured in acenes-based OSMs also depict only a low density of low energy modes.[20,41–44] Typically, FTIR covers a much narrower energy range because of limits in detectors. Recently, Schweicher et al. utilized Terahertz spectroscopy to access those lower energies in related OSMs to compare with the calculated phonons, but the limited number of resolved modes led to an average over-calculation of μ_hs by a factor of $\sim 3\times$.[21] We conclude that experimental validation solely with optical techniques such as Raman, FTIR, or THz spectroscopies, can lead to simulations that under-sample the phonon modes that are critical for charge transport. By comparison, we previously showed that validation to INS alone reproduces experimental μ_hs[16] because all of the modes over the full energy range and FBZ are sampled. Finally, we note that polarized Raman spectroscopy on single crystals can provide critical information about the anisotropy of polaron states[20,41] that is impossible to directly probe using INS.

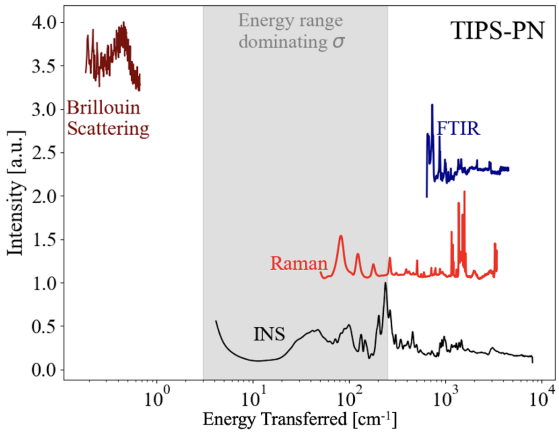

Figure 1: Comparison of experimental INS (black), Raman (red), FTIR (blue), and Brillouin scattering (maroon) spectra for TIPS-Pentacene.

Unlike optical-based spectroscopy, INS has been rarely utilized[45] to study the dynamics in OSCs.[46–48] Although low energy Raman has been used to differentiate the phases present in OSMs,[49] INS, specifically performed at the VISION spectrometer at Oak Ridge National Laboratory (ORNL), is currently the only instrument that can quantitatively resolve the phonon spectrum over both the entire vibrational energy range (5-5000 cm^{-1}) and k-space. VISION has a spectral brightness two orders of magnitude larger than that of similar instruments. Also other INS spectrometers are limited to either higher or lower energy ranges.[21,50–53]

This study compares INS spectra from a well known set of three substituted acenes, Fig. S2, that share similar brick-wall type stacking. We first compare these to each other and will then follow a similar analysis for herringbone packed materials. Our hope in studying similar structures is to determine whether particular features or trends relating to particular vibrational modes can assist in high μ_h OSC design. The substituted acenes, TIPS-Pentacene, TESADT, and diF-TESADT, exhibit respective increases in μ_h after molecular and chemical variations on the conjugated core and side-chains. Firstly, benzenes on the terminal ends of the conjugated core in TIPS-Pentacene (Fig. S2 top-left) are replaced with thiophenes, and a methyl group is removed from each branch of the side chain creating TESADT (Fig. S2

top-center). Previous research concluded that the sulfur-sulfur interactions provide stability between adjacent neighboring molecules,[54] with an increase in μ_h believed to arise from damped long-axis intermolecular motions.[55] Secondly, fluorines replaced a hydrogen atom on each thiophene along the long-axis of the backbone on TESADT, makes diF-TESADT (Fig. S2 top-right). This substitution further increased μ_h. It was reported that C-F polar covalent bonds and S-F dipoles,[56] and H-F hydrogen bonding[57] dampen the long-axis phonon further.

The measured and modeled spectra for the series of brick-wall type acenes are shown in Fig. 2, narrowed to 1500 cm^{-1} for clarity, with the full spectra shown in Fig. S3. We have previously demonstrated excellent experimental agreement with μ_h predictions based on INS measurements and modeled spectra.[16] The DFT model accurately resolves both the atomic positions and cell dimensions from diffraction experiments, and the atomic dynamics from INS over three-orders of energy. The excellent agreement between predicted and measured phonon modes provides a quantitative measure of the computed σ. Table 1 shows a comparison of the Γ-point and FBZ simulated μ_hs. The predicted μ_h are slightly overestimated because μ_h was measured over a large area that includes grain boundaries and defects in the crystal that are too long range for a periodic DFT simulation.

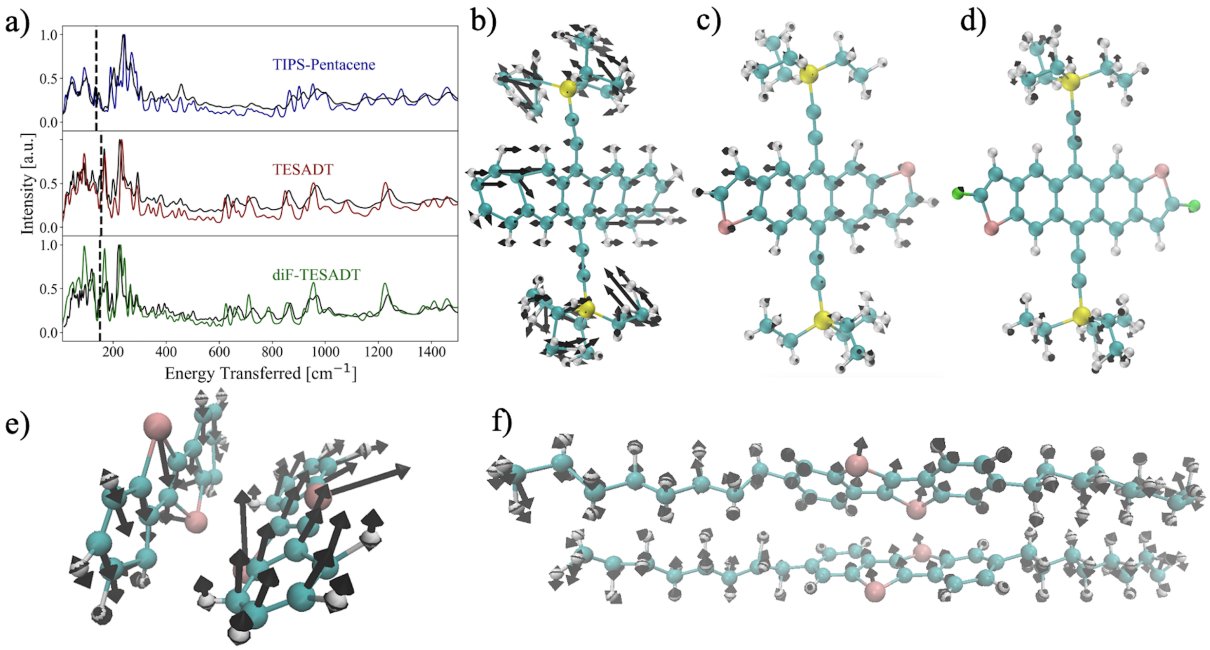

Figure 2: a) Experimental INS spectra in solid black for b) TIPS-Pentacene, c) TESADT, and d) diF-TESADT with corresponding optPBE-vdw simulated INS spectra in colored lines. Energy range is from 10-1500 cm^{-1}. Dashed vertical lines in a) highlight the phonon modes shown in b-d with frequencies 136, 155, and 150 cm^{-1}, respectively. Phonon eigenvectors are scaled by 5 for TIPS-Pentacene and 20 for TESADT and diF-TESADT to improve clarity. b-d highlights the effect of chemical change to the molecule on a single series of phonon modes with sizably altered transfer integrals. e-f highlights the modes at 45 and 50 cm^{-1} for BTBT and C8-BTBT, respectively, that show reduced phonon amplitudes.

Table 1 showcases a quantitative comparison between simulations. The Γ-point simulation could be validated by optical techniques (FTIR and Raman) but includes all modes, not just those allowed by selection rules. By comparison, INS spectroscopy includes the FBZ phonons and all modes. The experimental and computed spectra for FTIR and Raman of TIPS-Pentacene can be seen in Figs. S4 and S5, respectively. We show overall very good experimental agreement with most peaks present and the modes shifted by not more than 15 cm^{-1} (note Raman was recorded at room temp so the shift was expected). The Γ-point phonons were also experimentally validated against both FTIR and Raman, but computed μ_h is larger than for the FBZ calculations by over 100% in the worse case because many phonon modes are missing from the Γ-point analysis. Even when calculating σ at

the Γ-point, we found that no single phonon mode is responsible for more than 10% of σ, supporting a similar conclusion from a previous study.[53]

A convenient way to visualize the contribution of σ is by plotting the spectral density of electron-phonon coupling, as seen in Fig. S6 for TIPS-Pentacene and TESADT. The INS spectra are overlaid with the spectral density in Fig. S7, which shows which phonon modes make a large contribution to σ in the low energy region. Fig. S8 depicts a number of these phonon modes for TIPS-Pentacene from 20 to 150 cm^{-1} and clearly shows that most of these modes do not involve long-axis motions. Only the modes shown in Figs. S8b and S8c are Γ-point phonons, and therefore observable using optical measurements. As can be seen, considering only Γ-point phonons may skew the assessment of σ by leaving out modes that contribute to σ.

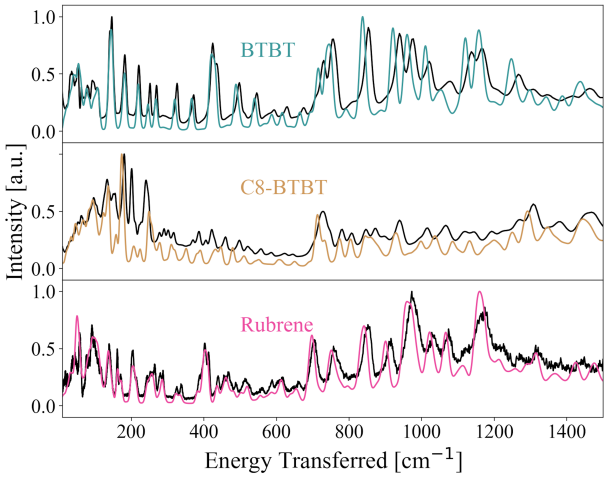

Figure 3: a) Experimental INS spectra in solid black for BTBT, C8-BTBT, and Rubrene with corresponding optPBE-vdw simulated INS spectra in colored lines. Energy range is from 10-1500 cm^{-1}.

By following a single energy equivalent series of phonon modes, it is possible to chart some of the effects that making a chemical change to the molecules can have on the dynamics. TIPS-Pentacene has a twist mode for the acene rings at 136 cm^{-1} depicted in Fig. 2b. Substituting to an ADT core replaces phenyl rings for end ring thiophenes, which has the effect of stiffening the ring structure and reducing the amplitude of the twisting mode in

TESADT (Fig. 2c). The modes depicted as delta functions in Fig. S7 are shown as molecular pictures in Figs. S8 and S9. The absolute magnitude of carbon motions in the backbone are reduced in TESADT while the sulfur amplitude is large due to the weak C–S bonds (Fig. S9d). The total σ in TESADT is lower than for TIPS-Pentacene because there are changes to a variety of modes that combine to reduce the total σ. Further comparing TESADT to diF-TESADT, the addition of a fluorine dampens out-of-plane sulfur motions and maintains the stiffened backbone as shown in Fig. 2d, with other relevant phonons shown in Fig. S10. We demonstrate that twisting, rotational, or rocking modes that are not along the long-axis can also cause small dynamic changes that have a clear affect on σ and contribute to the simulation of μ_h.

We now perform a similar analysis on BTBT, C8-BTBT, and Rubrene, with the INS spectra and spectral densities of electron-phonon coupling shown in Fig. 3 and S11, respectively. The spectral densities (S) are computed as explained in Ref. 16. BTBT, C8-BTBT, and Rubrene are much less structurally identical than the acenes, which makes a direct comparison across similar motions at similar energies impossible. Furthermore, C8-BTBT exhibits a low temperature polymorphism, while DFT was performed on the room temperature polymorph, leading to poor spectral agreement, particularly above $\sim$200 cm^{-1}. Nevertheless, the simulated phonons should still provide rough insight into the molecular structure and charge transport relationship. Thus we analyze the change in modes that contribute to σ from addition of the C8 side chains on BTBT (Figs. S12 and S13), and the significant modes for Rubrene shown in Figure S14. We see that each material contains many peaks in S over a broad range of energy implying that many different phonon modes contribute to the dynamic disorder. In these spectra, the peaks in high energy (e.g. around 1500 cm-1) are also due to carbon–carbon stretch modes as also noted in previous studies.

As can be seen, there are -9% to 28% relative changes between σ computed using the FBZ phonons and those of only Γ-point phonons. In substituted BTBT, there is a decrease in σ from including the phonon dispersion, which may seem counter-intuitive, but can be

explained by the improved convergence of the low frequency lattice modes.[33,58] Therefore, one can conclude that methods such as Raman and FTIR spectroscopy that are designed to only probe Γ-point phonons do not contain enough information to reliably parametrize the nonlocal electron-phonon coupling in these materials. An important notable point is that σ in C8-BTBT is smaller than those of BTBT itself in spite of the reduced order and higher flexibility of alkane bonds. As discussed in recent studies, the attachment of the side chains can shift the vibration range of the conjugated core toward higher frequencies that cannot be as easily populated at room temperature and accordingly do not effectively contribute as effectively to σ.[18,21] Accordingly, in the calculation of μ_h for C8-BTBT, only the contribution of low frequency modes in σ is considered. The computed μ_h of C8-BTBT, however, tends to be slightly smaller than those reported previously. This can be understood based on the fact that σ in this molecule changes in both directions (as can be seen in Table 1) and that the effect on μ_h goes from negligible in one direction to a factor of 2 in the other. This means that it is an effect that cannot be described by some systematic correction.

The μ_hs computed using the full phonon spectra for Rubrene and BTBT are smaller than those computed with only Γ-point phonons. The trend is more pronounced in Rubrene where also there is a considerable difference between σ associated to its largest transfer integral (pair A). This behavior is consistent with the rule proposed in Ref. 21 which expects the mobility to be scaled by $\mu\ \alpha\ (\sigma/\mathrm{J})^{\gamma}$ with $\gamma \approx$ "2" and those of Ref. 59 which predicts a rank correlation of up to $\sim$ -0.45 between σ and μ_h. Furthermore, it has been shown that organic field-effect transistors commonly are erroneously used to extract μs much higher than their true intrinsic value.[60]

A partial mode analysis is shown in Figs. S12-14 for BTBT, C8-BTBT, and Rubrene, respectively, which highlights the motions with sizable σ. BTBT has a large number of modes contributing to σ, including translation, flexing, and twisting. We again notice large amplitude sulfur motions from the weak C–S bonds arising consistently in the modes with energies above pure translation. For substituted BTBT, the long-axis mode shown in Fig.

S13a does indeed have an appreciable contribution to σ, but there are many other modes that are as much so or more impactful that should not be overlooked, as supported in Fig. S11c and S11d. The motions in substituted BTBT are similar to its unsubstituted analogue, but the addition of the long C8 side chains appear to lock in neighboring molecules resulting in reduced amplitude in overall displacements and noticeably of the sulfur motions, highlighted in Figs. 2e and 2f. For Rubrene, we again see opposing axial translation contributing to σ in Figs. S14a and S14b, wherein the phenyl rings reduce the amplitude of axial translation motions. At increasing energies, the weak C–C single bonds connecting the phenyl rings to the tetracene core allow large displacements with complex motions in the phenyl rings, including twisting and flapping. This in turn elicits a dampening response from the core resulting in its own twisting, bowing, and other motions. Overall, it is apparent that regardless of crystal packing, all motions within the conjugated well that contains the polaron contribute to σ.

Table 1: Computed parameters for the organic small molecules. Top row for each material are for pairs A and bottom row is pairs B for brick-wall type materials and pairs B and C for herringbone type materials. List of materials, transfer integrals J [meV], molecular pairs, band renormalization factor f, local dynamic disorder σ_{local} [meV], non-local dynamic disorder calculated considering only gamma point phonons σ_Γ [meV] and full Brillouin zone phonons σ_{FBZ} [meV] at 300 K, and respective mobilities [cm^2/Vs] computed in the framework of transient localization theory along with average experimental mobilities [cm^2/Vs]. μ_{exp} for TESADT and diF-TESADT consist of pure isomers in *anti* configuration. DFT calculations were also done on *anti* configurations.

Material	J	f	σ_{local}	σ_Γ	σ_{FBZ}	μ_Γ	μ_{FBZ}	μ_{exp}
diF-TESADT	-198.87	0.59	0.016	40.05	47.54	2.27	2.15	2.2 ± 1.1[57]
	-49.66			22.84	24.27			
TESADT	-172.01	0.61	0.016	43.65	57.13	2.03	1.87	1.2 ± 0.2[36]
	-59.09			27.91	30.14			
TIPS-PN	69.78	0.55	0.011	33.72	43.53	1.06	0.81	0.65 ± 0.35[35]
	1.96			15.22	15.98			
BTBT	113.58	0.43	0.015	30.00	32.28	0.86	0.82	0.024 ± 0.007[61]
	13.26			77.65	81.91			
C8-BTBT	88.01	0.47	0.021	26.18	23.80	1.85	2.55	6.0 ± 1.1[61]
	-62.94			54.52	50.06			
Rubrene	147.87	0.65	0.018	36.40	50.64	8.73	4.01	9.25 ± 0.75[62]
	22.69			9.56	10.09			

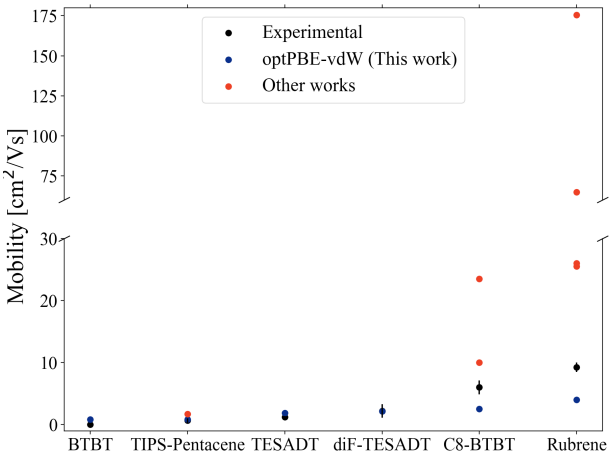

Figure 4: Average experimental (black) and theoretical (blue) μ_hs for the molecules used in this letter. Red marks are average μ_hs, in the high mobility plane where available, for other work with theories including TLT, Boltzmann transport based acoustic phonon deformation potential, time-dependent wavepacket diffusion, and quantum nuclear tunneling.[21,40,63,64]

In summary, application of TLT simulations combined with validated phonon modes can lead to accurate predictions of μ_h. For comparison sake, μ_h predictions in this work and other published predictions using several different theories are shown in Fig. 4. Here we address that the choice of validation data can affect the accuracy of these simulations by enabling measuring of either Γ-point or FBZ data. Accurate phonons allow for a sequential mode analysis probing the effect of minor chemical changes and σ significant phonons. Examination of the full phonon spectrum shows that many modes contribute to σ, without any mode contributing more than 10%, and so a design rule focusing on a single phonon mode is unlikely to drastically improve μ_h.

Looking forward, although the calculated μ_hs quantitatively reproduced measured μ_h, these FBZ phonon calculations are limited by the enormous computational expense of DFT. A typical calculation with a 100 atom unit cell costs $> 10^5$ CPU hours on a supercomputer per 2×2×1 supercell. Therefore we cannot model imperfections such as grain boundaries or structural/chemical defects. Furthermore, rapid screening of theoretical materials based on σ would not be feasible. To overcome this limitation, considerable attention has been focused on computationally cheaper methods. Recent examples include molecular dynamics

(MD),[65] density functional based tight binding (DFTB),[66,67] or a mixture such as quantum mechanics/molecular mechanics (QM/MM),[59] DFT-MD,[68] and ChIMES/DFTB.[31] Computationally demanding studies, such as this one, are essential as benchmarks for validating more approximate simulation methods.

Acknowledgement

This research was supported by the Department of Energy, Basic Energy Sciences, Award DE-SC0010419, including salary for D.V., M.D. and A.J.M. This research used resources of the National Energy Research Scientific Computing Center (NERSC), a DOE Office of Science User Facility supported by the Office of Science of the U.S. Department of Energy under Contract No. DE-AC02-05CH11231. The INS spectrum was measured at the Spallation Neutron Source, a DOE Office of Science User Facility operated by the Oak Ridge National Laboratory, partly supported by LLNL under Contract DE-AC52-07NA27344. J.E.A. was supported by the National Science Foundation, under cooperative agreement No. 1849213. TN and AT acknowledge the financial support from ERC (PoC grant No. 403098).

Supporting Information Available

Supporting Information Available:

Computational and experimental methodology for Brillouin scattering, Raman, FTIR, INS, and dynamic disorder and mobility, with respective unit cells, spectra, band structures, and relevant phonon modes.

References

(1) Shi, Y. L.; Zhuo, M. P.; Wang, X. D.; Liao, L. S. Two-Dimensional Organic Semiconductor Crystals for Photonics Applications. *ACS Applied Nano Materials* **2020**, *3*,

1080–1097.

(2) Zhang, X.; Dong, H.; Hu, W. Organic Semiconductor Single Crystals for Electronics and Photonics. *Advanced Materials* **2018**, *30*, 1–34.

(3) Schweicher, G.; Garbay, G.; Jouclas, R.; Vibert, F.; Devaux, F.; Geerts, Y. H. Molecular Semiconductors for Logic Operations: Dead-End or Bright Future? *Advanced Materials* **2020**, *32*, 1905909.

(4) Wang, N.; Yang, A.; Fu, Y.; Li, Y.; Yan, F. Functionalized Organic Thin Film Transistors for Biosensing. *Accounts of Chemical Research* **2019**, *52(2)*, 277–287.

(5) Qian, Y.; Zhang, X.; Xie, L.; Qi, D.; Chandran, B. K.; Chen, X.; Huang, W. Stretchable Organic Semiconductor Devices. *Advanced Materials* **2016**, *28*, 9243–9265.

(6) Wang, Y.; Sun, L.; Wang, C.; Yang, F.; Ren, X.; Zhang, X.; Dong, H.; Hu, W. Organic crystalline materials in flexible electronics. *Chemical Society Reviews* **2019**, *48*, 1492–1530.

(7) Wang, C.; Dong, H.; Jiang, L.; Hu, W. Organic semiconductor crystals. *Chemical Society Reviews* **2018**, *47*, 422–500.

(8) Horowitz, G.; Hajlaoui, M. E.; Hajlaoui, R. Temperature and gate voltage dependence of hole mobility in polycrystalline oligothiophene thin film transistors. *Journal of Applied Physics* **2000**, *87*, 4456–4463.

(9) Kalb, W. L.; Haas, S.; Krellner, C.; Mathis, T.; Batlogg, B. Trap density of states in small-molecule organic semiconductors: A quantitative comparison of thin-film transistors with single crystals. *Physical Review B - Condensed Matter and Materials Physics* **2010**, *81*, 1–13.

(10) Anthony, J. E.; Brooks, J. S.; Eaton, D. L.; Parkin, S. R.; May, R. V. Functionalized

Pentacene: Improved Electronic Properties from Control of Solid-State Order. **2001**, *222*, 1–2.

(11) Payne, M. M.; Odom, S. A.; Parkin, S. R.; Anthony, J. E. Stable, crystalline acenedithiophenes with up to seven linearly fused rings. *Organic Letters* **2004**, *6*, 3325–3328.

(12) Jurchescu, O. D.; Baas, J.; Palstra, T. T. Effect of impurities on the mobility of single crystal pentacene. *Applied Physics Letters* **2004**, *84*, 3061–3063.

(13) Subramanian, S.; Sung, K. P.; Parkin, S. R.; Podzorov, V.; Jackson, T. N.; Anthony, J. E. Chromophore fluorination enhances crystallization and stability of soluble anthradithiophene semiconductors. *Journal of the American Chemical Society* **2008**, *130*, 2706–2707.

(14) Wo, S.; Headrick, R. L.; Anthony, J. E. Fabrication and characterization of controllable grain boundary arrays in solution-processed small molecule organic semiconductor films. *Journal of Applied Physics* **2012**, *111*, 073716.

(15) Illig, S.; Eggeman, A. S.; Troisi, A.; Jiang, L.; Warwick, C.; Nikolka, M.; Schweicher, G.; Yeates, S. G.; Henri Geerts, Y.; Anthony, J. E. et al. Reducing dynamic disorder in small-molecule organic semiconductors by suppressing large-Amplitude thermal motions. *Nature Communications* **2016**, *7*, 1–10.

(16) Harrelson, T. F.; Dantanarayana, V.; Xie, X.; Koshnick, C.; Nai, D.; Fair, R.; Nuñez, S. A.; Thomas, A. K.; Murrey, T. L.; Hickner, M. A. et al. Direct probe of the nuclear modes limiting charge mobility in molecular semiconductors. *Materials Horizons* **2019**, *6*, 182–191.

(17) Fratini, S.; Ciuchi, S.; Mayou, D.; De Laissardière, G. T.; Troisi, A. A map of high-mobility molecular semiconductors. *Nature Materials* **2017**, *16*, 998–1002.

(18) Nematiaram, T.; Troisi, A. Strategies to reduce the dynamic disorder in molecular semiconductors. *Materials Horizons* **2020**, *7*, 2922–2928.

(19) Fratini, S.; Nikolka, M.; Salleo, A.; Schweicher, G.; Sirringhaus, H. Charge transport in high-mobility conjugated polymers and molecular semiconductors. *Nature Materials* **2020**, *19*, 491–502.

(20) Bittle, E. G.; Biacchi, A. J.; Fredin, L. A.; Herzing, A. A.; Allison, T. C.; Hight Walker, A. R.; Gundlach, D. J. Correlating anisotropic mobility and intermolecular phonons in organic semiconductors to investigate transient localization. *Communications Physics* **2019**, *2*, 29.

(21) Schweicher, G.; D'Avino, G.; Ruggiero, M. T.; Harkin, D. J.; Broch, K.; Venkateshvaran, D.; Liu, G.; Richard, A.; Ruzié, C.; Armstrong, J. et al. Chasing the "Killer" Phonon Mode for the Rational Design of Low-Disorder, High-Mobility Molecular Semiconductors. *Advanced Materials* **2019**, *31*, 1902407.

(22) Ortmann, F.; Bechstedt, F.; Hannewald, K. Charge transport in organic crystals: Theory and modelling. *Physica Status Solidi (B) Basic Research* **2011**, *248*, 511–525.

(23) Blumberger, J. Recent Advances in the Theory and Molecular Simulation of Biological Electron Transfer Reactions. *Chemical Reviews* **2015**, *115*, 11191–11238.

(24) Giannini, S.; Carof, A.; Ellis, M.; Yang, H.; Ziogos, O. G.; Ghosh, S.; Blumberger, J. Quantum localization and delocalization of charge carriers in organic semiconducting crystals. *Nature Communications* **2019**, *10*, 1–12.

(25) Wang, L.; Prezhdo, O. V.; Beljonne, D. Mixed quantum-classical dynamics for charge transport in organics. *Physical Chemistry Chemical Physics* **2015**, *17*, 12395–12406.

(26) Heck, A.; Kranz, J. J.; Kubař, T.; Elstner, M. Multi-scale approach to non-adiabatic

charge transport in high-mobility organic semiconductors. *Journal of Chemical Theory and Computation* **2015**, *11*, 5068–5082.

(27) Jiang, Y.; Geng, H.; Li, W.; Shuai, Z. Understanding Carrier Transport in Organic Semiconductors: Computation of Charge Mobility Considering Quantum Nuclear Tunneling and Delocalization Effects. *Journal of Chemical Theory and Computation* **2019**, *15*, 1477–1491.

(28) Ruggiero, M. T.; Ciuchi, S.; Fratini, S.; D'Avino, G. Electronic Structure, Electron-Phonon Coupling, and Charge Transport in Crystalline Rubrene under Mechanical Strain. *Journal of Physical Chemistry C* **2019**, *123*, 15897–15907.

(29) Ren, X.; Bruzek, M. J.; Hanifi, D. A.; Schulzetenberg, A.; Wu, Y.; Kim, C. H.; Zhang, Z.; Johns, J. E.; Salleo, A.; Fratini, S. et al. Negative Isotope Effect on Field-Effect Hole Transport in Fully Substituted 13C-Rubrene. *Advanced Electronic Materials* **2017**, *3*, 1–7.

(30) Nematiaram, T.; Ciuchi, S.; Xie, X.; Fratini, S.; Troisi, A. Practical Computation of the Charge Mobility in Molecular Semiconductors Using Transient Localization Theory. *Journal of Physical Chemistry C* **2019**, *123*, 6989–6997.

(31) Dantanarayana, V.; Nematiaram, T.; Vong, D.; Anthony, J. E.; Troisi, A.; Nguyen Cong, K.; Goldman, N.; Faller, R.; Moulé, A. J. Predictive Model of Charge Mobilities in Organic Semiconductor Small Molecules with Force-Matched Potentials. *Journal of Chemical Theory and Computation* **2020**, *16*, 3494–3503.

(32) Landi, A. Charge Mobility Prediction in Organic Semiconductors: Comparison of Second-Order Cumulant Approximation and Transient Localization Theory. *Journal of Physical Chemistry C* **2019**, *123*, 18804–18812.

(33) Tu, Z.; Yi, Y.; Coropceanu, V.; Brédas, J. L. Impact of Phonon Dispersion on Nonlocal

Electron-Phonon Couplings in Organic Semiconductors: The Naphthalene Crystal as a Case Study. *Journal of Physical Chemistry C* **2018**, *122*, 44–49.

(34) Nematiaram, T.; Troisi, A. Modeling charge transport in high-mobility molecular semiconductors: Balancing electronic structure and quantum dynamics methods with the help of experiments. *Journal of Chemical Physics* **2020**, *152*, 190902.

(35) Park, S. K.; Jackson, T. N.; Anthony, J. E.; Mourey, D. A. High mobility solution processed 6,13-bis(triisopropyl-silylethynyl) pentacene organic thin film transistors. *Applied Physics Letters* **2007**, *91*, 6–9.

(36) Hailey, A. K.; Petty, A. J.; Washbourne, J.; Thorley, K. J.; Parkin, S. R.; Anthony, J. E.; Loo, Y. L. Understanding the Crystal Packing and Organic Thin-Film Transistor Performance in Isomeric Guest–Host Systems. *Advanced Materials* **2017**, *29*, 1–8.

(37) Jurchescu, O. D.; Subramanian, S.; Kline, R. J.; Hudson, S. D.; Anthony, J. E.; Jackson, T. N.; Gundlach, D. J. Organic single-crystal field-effect transistors of a soluble anthradithiophene. *Chemistry of Materials* **2008**, *20*, 6733–6737.

(38) Fratini, S.; Mayou, D.; Ciuchi, S. The Transient Localization Scenario for Charge Transport in Crystalline Organic Materials. **2016**, *26*, 2292–2315.

(39) Charge-transport regime of crystalline organic semiconductors: Diffusion limited by thermal off-diagonal electronic disorder. *Physical Review Letters* **2006**, *96*, 1–4.

(40) Shuai, Z.; Li, W.; Ren, J.; Jiang, Y.; Geng, H. Applying Marcus theory to describe the carrier transports in organic semiconductors: Limitations and beyond. *Journal of Chemical Physics* **2020**, *153*, 080902–7–080902–11.

(41) Asher, M.; Angerer, D.; Korobko, R.; Diskin-Posner, Y.; Egger, D. A.; Yaffe, O. Anharmonic Lattice Vibrations in Small-Molecule Organic Semiconductors. *Advanced Materials* **2020**, *32*, 1908028.

(42) Brillante, A.; Bilotti, I.; Della Valle, R. G.; Venuti, E.; Girlando, A. Probing polymorphs of organic semiconductors by lattice phonon Raman microscopy. *CrystEngComm* **2008**, *10*, 937–946.

(43) Weinberg-Wolf, J. R.; McNeil, L. E.; Liu, S.; Kloc, C. Evidence of low intermolecular coupling in rubrene single crystals by Raman scattering. *Journal of Physics Condensed Matter* **2007**, *19*, 276204.

(44) Sosorev, A. Y.; Maslennikov, D. R.; Kharlanov, O. G.; Chernyshov, I. Y.; Bruevich, V. V.; Paraschuk, D. Y. Impact of Low-Frequency Vibrations on Charge Transport in High-Mobility Organic Semiconductors. *Physica Status Solidi - Rapid Research Letters* **2019**, *13*, 1–23.

(45) Cavaye, H. Neutron Spectroscopy: An Under-Utilised Tool for Organic Electronics Research? *Angewandte Chemie - International Edition* **2019**, *58*, 9338–9346.

(46) Pintschovius, L.; Rietschel, H.; Sasaki, T.; Mori, H.; Tanaka, S.; Toyota, N.; Lang, M.; Steglich, F. Observation of superconductivity-induced phonon frequency changes in the organic superconductor κ-(BEDT-TTF)2Cu(NCS)2. *Europhysics Letters* **1997**, *37*, 627–632.

(47) Degli Esposti, A.; Moze, O.; Taliani, C.; Tomkinson, J. T.; Zamboni, R.; Zerbetto, F. The intramolecular vibrations of prototypical polythiophenes. *Journal of Chemical Physics* **1996**, *104*, 9704–9718.

(48) Hermet, P.; Bantignies, J. L.; Rahmani, A.; Sauvajol, J. L.; Johnson, M. R. Polymorphism of crystalline α-quaterthiophene and α-sexithiophene: Ab initio analysis and comparison with inelastic neutron scattering response. *Journal of Physical Chemistry A* **2005**, *109*, 4202–4207.

(49) Bedoya-Martínez, N.; Schrode, B.; Jones, A. O.; Salzillo, T.; Ruzié, C.; Demitri, N.; Geerts, Y. H.; Venuti, E.; Della Valle, R. G.; Zojer, E. et al. DFT-Assisted Polymorph

Identification from Lattice Raman Fingerprinting. *Journal of Physical Chemistry Letters* **2017**, *8*, 3690–3695.

(50) Hermet, P.; Lois-Sierra, S.; Bantignies, J. L.; Rols, S.; Sauvajol, J. L.; Serein-Spirau, F.; Lère-Porte, J. P.; Moreau, J. J. Lattice dynamics of oligo(phenylenethienylene)s: A far-infrared and inelastic neutron scattering study. *Journal of Physical Chemistry B* **2009**, *113*, 4197–4202.

(51) Guilbert, A. A.; Parr, Z. S.; Kreouzis, T.; Woods, D. J.; Sprick, R. S.; Abrahams, I.; Nielsen, C. B.; Zbiri, M. Effect of substituting non-polar chains with polar chains on the structural dynamics of small organic molecule and polymer semiconductors. *Physical Chemistry Chemical Physics* **2021**, *23*, 7462–7471.

(52) Kruglova, O.; Mulder, F. M.; Kotlewski, A.; Picken, S. J.; Parker, S.; Johnson, M. R.; Kearley, G. J. A compact model system for electron-phonon calculations in discotic materials. *Chemical Physics* **2006**, *330*, 360–364.

(53) Stoeckel, M.-A.; Oliver, Y.; Gobbi, M.; Dudenko, D.; Lemaur, V.; Zbiri, M.; Guilbert, A. A. Y.; D'Avino, G.; Liscio, F.; Migliori, A. et al. Analysis of External and Internal Disorder to Understand Band-Like Transport in n-Type Organic Semiconductors. *Advanced Materials* **2021**, *33*, 2007870.

(54) Wang, Y.; Parkin, S. R.; Gierschner, J.; Watson, M. D. Benzobisbenzothiophenes. **2008**, *10 (15)*, 3307—-3310.

(55) Eggeman, A. S.; Illig, S.; Troisi, A.; Sirringhaus, H.; Midgley, P. A. Measurement of molecular motion in organic semiconductors by thermal diffuse electron scattering. *Nature Materials* **2013**, *12*, 1045–1049.

(56) Thorley, K. J.; McCulloch, I. Why are S-F and S-O non-covalent interactions stabilising? *Journal of Materials Chemistry C* **2018**, *6*, 12413–12421.

(57) Hallani, R. K.; Thorley, K. J.; Mei, Y.; Parkin, S. R.; Jurchescu, O. D.; Anthony, J. E. Structural and electronic properties of crystalline, isomerically pure anthradithiophene derivatives. *Advanced Functional Materials* **2016**, *26*, 2341–2348.

(58) Kamencek, T.; Zojer, E. Discovering structure–property relationships for the phonon band structures of hydrocarbon-based organic semiconductor crystals: the instructive case of acenes. *Journal of Materials Chemistry C* **2022**, *10*, 2532–2543.

(59) Nematiaram, T.; Padula, D.; Landi, A.; Troisi, A. On the Largest Possible Mobility of Molecular Semiconductors and How to Achieve It. *Advanced Functional Materials* **2020**, *30*, 1–10.

(60) Choi, H. H.; Cho, K.; Frisbie, C. D.; Sirringhaus, H.; Podzorov, V. Critical assessment of charge mobility extraction in FETs. *Nature Materials* **2017**, *17*, 2–7.

(61) Adhikari, J.; Zhan, P.; Calitree, B.; Zhang, W.; Fair, R.; Harrelson, T.; Faller, R.; Moule, A.; Milner, S.; Maranas, J. et al. Side chain addition suppresses lattice fluctuations and enhances charge mobilities in benzothienobenzothiophenes. submitted 2021.

(62) Menard, E.; Podzorov, V.; Hur, S. H.; Gaur, A.; Gershenson, M. E.; Rogers, J. A. High-performance n- And p-type single-crystal organic transistors with free-space gate dielectrics. *Advanced Materials* **2004**, *16*, 2097–2101.

(63) Kobayashi, H.; Kobayashi, N.; Hosoi, S.; Koshitani, N.; Murakami, D.; Shirasawa, R.; Kudo, Y.; Hobara, D.; Tokita, Y.; Itabashi, M. Hopping and band mobilities of pentacene, rubrene, and 2,7-dioctyl[1] benzothieno[3,2-b][1]benzothiophene (C8-BTBT) from first principle calculations. *Journal of Chemical Physics* **2013**, *139*, 1132–1133.

(64) Geng, H.; Peng, Q.; Wang, L.; Li, H.; Liao, Y.; Ma, Z.; Shuai, Z. Toward quantitative prediction of charge mobility in organic semiconductors: Tunneling enabled hopping model. *Advanced Materials* **2012**, *24*, 3568–3572.

(65) Pelzer, K. M.; Vázquez-Mayagoitia, Á.; Ratcliff, L. E.; Tretiak, S.; Bair, R. A.; Gray, S. K.; Van Voorhis, T.; Larsen, R. E.; Darling, S. B. Molecular dynamics and charge transport in organic semiconductors: a classical approach to modeling electron transfer. *Chemical Science* **2017**, *8*, 2597–2609.

(66) Landi, A.; Troisi, A. Rapid Evaluation of Dynamic Electronic Disorder in Molecular Semiconductors. *Journal of Physical Chemistry C* **2018**, *122*, 18336–18345.

(67) Xie, X.; Santana-Bonilla, A.; Troisi, A. Nonlocal Electron-Phonon Coupling in Prototypical Molecular Semiconductors from First Principles. *Journal of Chemical Theory and Computation* **2018**, *14*, 3752–3762.

(68) Harrelson, T. F.; Dettmann, M.; Scherer, C.; Andrienko, D.; Moulé, A. J.; Faller, R. Computing inelastic neutron scattering spectra from molecular dynamics trajectories. *Scientific Reports* **2021**, *11*, 1–12.